PCCP

Accepted Manuscript

ROYAL SOCIETY OF CHEMISTRY

www.rsc.org/pccp

Morphological Effect of Gold Nanoparticle on the Adsorption of Bovine Serum Albumin

Abhishek Chaudhary, Abhishek Gupta, Syamantak Khan, and Chayan Kanti Nandi *

School of Basic Sciences, Indian Institute of Technology Mandi, Himachal Pradesh, India-175001

Corresponding author

*Chayan K. Nandi

School of Basic Sciences,

Indian Institute of Technology Mandi,

Himachal Pradesh-175001, India

Email: chayan@iitmandi.ac.in

KEYWORDS: gold nanoparticles, morphology, protein monolayer, bovine serum albumin, docking simulation.

Abstract:

Various properties of gold nanoparticles (GNPs) are found to play crucial roles in their biological activity. Among them, the morphology and the surface chemistry are extremely important. This is because of differences in surface energies of various crystal facets arising from a large fraction of edges, corners and vertices. In the present work, we provide a comparative study on the adsorption and binding affinities of bovine serum albumin (BSA) onto triangular gold nanoplate (TGNP) and gold nanorod (GNR). The results were compared with similar size of both CTAB and citrate stabilized spherical GNPs. Our data suggested stronger binding of BSA on a citrate stabilized spherical GNPs whereas TGNP shows the weakest binding among all the GNPs. Approximately 20 nm blue shifting in tryptophan fluorescence was observed for all CTAB stabilized GNPs, suggesting the local dielectric changes surrounding tryptophan residue. Secondary structural loss was also observed for all CTAB stabilized GNPs. No spectral shift was observed for citrate stabilized spherical GNPs though maximum quenching of fluorescence and minimum structural loss was observed for it. With the help of recently developed molecular simulation in our group, a binding model is proposed to explain all the above experimental results.

1. Introduction:

Elucidating the nature of protein adsorption on the nanoparticle surface is extremely important because of the formation of protein corona around the metal surface when it enters into the biological fluid. This corona, finally, determines the fate and the biological activity of the nanoparticle. It immensely hampers the targeting capability and efficiency of specific delivery in an actual *in-vivo* environment.[1-3] Most of the nanoparticles bind to an array of proteins to form both soft (weakly bound) and hard corona (tightly bound proteins).[4-5] However, it is extremely difficult to establish any specific rules that govern the adsorption and conformation of adsorbed biomolecules on nanoparticle surface. This gets further complicated by the diversity of protein structures and their various possible orientations. Because of the associative nature of the common blood proteins with nanoparticles, blood viscosity and clotting property associated with the nanoparticle conjugation changes substantially. This in turn influences various physiological changes causing serious health risk.[6]

On the other hand, for the dynamic nature of adsorption on metal surface, protein can attach, detach, or rearrange its conformations and co-adsorbed with of other ions and proteins within that time scale. These structural changes in protein native state expose new epitopes on the protein surface[7] or perturb the normal protein function[8] and alter the bio-distribution, cellular uptake mechanism, and intracellular location of nanoparticle i*n-vivo*.[1-3] A general trend is suggested that the lower curvature of nanoparticle causes more perturbation of the protein structure, however this may not be universally true.[9-11] For instance, 2D self-assembled monolayers (SAM) of a polypeptide chain gets more distorted on a surface with increasing radius at around 20 nm, while remains stable with increasing the particle size close to a flat surface.[12]

On the other hand, serum albumin loses its secondary structure on a larger nanoparticle whereas fibrinogen remains stable.[13] These contradictory observations is difficult to explain with the existing knowledge of protein adsorption and further its orientation onto the nanoparticle surface. It is also worth mentioning the difficulties in correlating the protein nanoparticle interaction to real bio-corona formation.[1,14] However, the in depth knowledge of the protein adsorption at the molecular level could help in understanding the function of the Nano bio conjugate. Hence, understanding the protein nanoparticle interaction is extremely important which will allow the rational design for target specific drug delivery and tissue engineering.[15-20]

Among the various properties, the morphology and the surface chemistry of nanoparticles are extremely important because of the difference in surface energies that arises from a large fraction of edges, corners, vertices and particle curvature.[21-25] Among various GNPs, GNR has been extensively studied for its biological activities like cancer imaging and tumor ablation.[26-28] However, little attention has been paid on TGNP, though the potential for its bio application, especially in tissue, is also equally important due to the presence of SPR band in the NIR region.[29-32] The deep penetration of radiation can be improved by minimizing photon absorption of tissue components as in this region it doesn't have any absorption. Moreover, both the anisotropic GNPs can act as Nano-heaters for remote ablation of tumors using NIR radiation.[26-32]

In the present work, we are providing a comparative study on the morphological effect of GNP with different shapes and surface chemistries on the adsorption of BSA under the same experimental condition. BSA is the most widely utilized serum protein due to its low cost, wide availability and well-known structure **(Supporting Figure S1).**[33] It is a single polypeptide chain with 583 amino acid residues with a molecular weight of 66.4 kDa.[34] The secondary structure purportedly contains roughly 67% α-helix structure.[35] The tertiary structure consists of nine

loops stabilized by 17 internal disulfide bonds between 34 cysteine residues, resulting in three primary domains, each containing one small and two large loops. These disulfide bridges are the basis for the compact heart-shaped (equilateral triangle) structure.[36,37] The fluorescence properties of two tryptophan moieties in two sub-domains (one on the surface and the other in the hydrophobic pocket) are exploited for studying the conformation changes of the protein in different environmental conditions.[38]

The synthesized TGNP edge length, GNR longitudinal length and the spherical GNPs all are around of 40nm in diameter. A wide range of photo physical techniques such as steady state and time resolved fluorescence, UV-Vis-NIR, Fourier Transformed Infrared Spectra **(**FTIR), Circular Dichroism (CD), Transmission Electron Microscope (TEM) and Dynamic light Scattering (DLS) were used for the experimental study. Along with fluorescence quenching, approximately 20nm blue shifting in tryptophan fluorescence was observed for all CTAB stabilized GNPs. Secondary structural loss was also observed for all CTAB stabilized GNPs. However, in citrate stabilized spherical GNP instead of any spectral shifting maximum quenching as well as strong binding was observed among all the GNPs. With the help of our recently developed molecular simulation techniques, a binding model is proposed to explain all the above experimental results.

2. Experimental

2.1 Materials and Methods

2.1.1 Materials: All the chemicals Gold (III) Chloride hydrate ($HAuCl_4.3H_2O$ 99.99%), Sodium Citrate tribasic hydrate (> 99%), Sodium Borohydride ($NaBH_4$, 99%), L- Ascorbic Acid were purchased from Sigma Aldrich. CTAB (N-Cetyl-N,N,N-trimethyl-ammonium bromide), Silver Nitrate ($AgNO_3$, 99.5%), Sodium Hydroxide Pellet purified (NaOH, 97%), were purchased from Merck and Sodium Iodide (NaI, 99%) was purchased from Fisher Scientific. BSA protein was

purchased from Sigma Aldrich. Double distilled 18.3 mΩ deionized water (Elga Pure lab Ultra) was used throughout the preparation of solutions. All glasswares were washed with aqua regia (3 HCl: 1 HNO_3), followed by rinsing with double distilled water for several times.

2.1.2 Synthesis of citrate stabilized spherical GNP: Citrate stabilized spherical GNP of 40 nm diameter was prepared by the seed mediated method.[39] 36.5ml deionized water taken in a conical flask and 0.5 ml of 10mM $HAuCl_4.3H_2O$ was added into it. The temperature was maintained at 40 °C. The mixture was vigorously stirred on a hot magnetic stirrer. 1 ml of 5mM aqueous solution of sodium citrate and 1 ml of 50mM $NaBH_4$ (Cold) solutions were added to the solution. The solution was then kept at room temperature with additional stirring for 10 minutes until the color of the solution turned from pale yellow to light Red. The resulting mixture was aged for 2-4 hour to allow the hydrolysis of unreacted $NaBH_4$.

2.1.3 Synthesis of CTAB stabilized spherical GNP: - CTAB stabilized spherical GNP was synthesized by using a seed-mediated growth method.[40] The container for seed synthesis held 5mL of 0.50mM $HAuCl_4.3H_2O$ and 5mL of 0.20 M CTAB. The solution was reduced by addition of 600μL of ice-cold $NaBH_4$ (0.010 M). Next, the container was shaken vigorously for 2 min and occasionally opened to vent for any evolved hydrogen gas. The seed solution was brown suspensions and was allowed to age for 2 hours. 12μL of seed solution had been to a solution already containing 9.50 mL of 0.10 M CTAB, 80μL of 0.010 M $AgNO_3$, 500μL of 0.010 M $HAuCl_4.3H_2O$ and 55μL of 0.10 M Ascorbic Acid. The mixture was stirred for 10min. This resulted in a red suspension that was again left undisturbed for 24 hours to increase the yield. The extra CTAB was removed by centrifugation and resuspension of the nanoparticle into equal amount of water.

2.1.4 Synthesis of TGNP: TGNP was synthesized by the established seed mediated method.[41] Approximately 5nm spherical seed was prepared by mixing 0.5mL of a 10mM aqueous $HAuCl_4.3H_2O$ solution, 1 mL of a 5mM aqueous solution of sodium citrate and 1mL of a 50mM aqueous $NaBH_4$ (Ice-cold) solution in 36.5 mL of deionized water. The solution was vigorous stirred till color of the solution turned into red. To prepare TGNP, three labeled (namely 1, 2 and 3) flasks were prepared. A mixture of 108 mL of 0.025M aqueous CTAB solution and 54μL of 0.05M aqueous NaI solutions was divided into the above three containers. 9 ml of mixture was added in each container 1 and 2. The remaining mixture 90 ml was added in container 3. Finally, a mixture of 125μL of a 10mM aqueous $HAuCl_4 \cdot 3H_2O$ solution, 50μL of 50mM NaOH, and 80μL of 50mM ascorbic acid was added to each container 1 and 2. A mixture of 1.25mL of 10mM $HAuCl_4 \cdot 3H_2O$, 0.5mL of 50mM NaOH, and 0.5mL of 50mM ascorbic acid was added to container 3. 1ml of the seed solution was added to container 1 with mild shaking, followed by addition of 1 ml of container 1 solution into container 2. After gentle shaking, the whole solution of container 2 was added to container 3. The solution was kept overnight and extra amount of CTAB was removed from the solution by centrifugation (5000 rpm for 10 minutes) followed by resuspension of the TGNP in water.

2.1.5 Synthesis of GNR: GNR was also synthesized using the seed mediated method. [42] Seeds were prepared by adding an aqueous ice-cold $NaBH_4$ solution (0.600 ml, 0.01 M) to a solution obtained by adding aqueous $HAuCl_4.3H_2O$ (0.250 mL, 0.01 M) to an aqueous solution of CTAB (7.5 mL, 0.10 M). The seed growth was allowed to grow for 2 hours. Next, an aliquot of the seed solution was added to a solution containing aqueous CTAB (95mL, 0.10 M), $HAuCl_4.3H_2O$ (4mL, 0.01 M), aqueous $AgNO_3$ (0.6mL, 0.01 M) and an aqueous ascorbic acid solution (0.64mL, 0.10 M). Immediately after the addition of seed solution, the mixture was stirred gently

for 10s. Finally, the solution was kept at 27 °C (in a water bath) undisturbed for at least 3 hours. The extra CTAB was removed by centrifugation (5000 rpm for 10 minutes) followed by resuspension in water.

2.2 Characterization of all synthesized GNPs: Particle size and dispersity of the synthesized nanoparticles were characterized by using a TECNAI 200 kV TEM (FEI, Electron Optics). The hydrodynamic diameter (D_H) and Zeta potential of the nanoparticles and their protein complexes were measured by DLS using Zeta Sizer Nano, equipped with a He Ne laser illumination at 633 nm in a single photon counting mode using avalanche photodiode for signal detection (Malvern Instrument).

2.3 Steady State and Time Resolved Fluorescence Spectroscopy:

Steady state fluorescence was measured using Agilent Spectrofluorometer (Carry Eclipse)**.** Fluorescence lifetime was measured by using ChronosBH fluorescence lifetime spectrometer (ISS, USA). Phosphate Buffer Saline (PBS buffer) was used for preparing the BSA solution. A 3 ml quartz cuvette was used for both the measurements. HORIBA 280nm Delta-Diode was used for time resolved measurements.

The decay curve was fitted using the following equation,

$$\boldsymbol{I(t) = \sum_i \alpha_i \, exp\left(\frac{-t}{\tau_i}\right)} \qquad [1]$$

Here, the initial intensity of the component i is α_i with lifetime τ. The average lifetime was calculated using the following equation,

$$\boldsymbol{\tau_m = \frac{\sum_i \alpha_i \tau_i}{\sum_i \alpha_i}} \qquad [2]$$

2.4 Quantum Yield, Radiative (k_R) and Nonradiative decay (k_{NR}) calculation:

Rhodamine 6G was used as standard for determining the quantum yield. The following equation was used for calculating the quantum yield[43]

$$\Phi = \frac{A_s F_u n_u^2}{A_u F_s n_s^2} \times \Phi_s \qquad [3]$$

Where A_s is the absorbance of Rhodamine 6G and A_u is the absorbance of unknown sample. $\mathbf{F_s}$ ***is*** the area under the curve of the fluorescence peak of Rhodamine 6G and F_u is the area under the curve of the fluorescence peak of unknown sample. n ($\mathbf{n_s = n_u}$) is refractive index of solvent and is equal to 1.33 for water**.** $\boldsymbol{\Phi_s}$ is the quantum yield of Rhodamine 6G. $\boldsymbol{\Phi_u}$ is the quantum yield of unknown sample.

The following equation was used to calculate the radiative and nonradiative decay rate constant[43].

$$k_{NR} = k_R \left[\frac{1}{\Phi} - 1\right] \qquad [4]$$

where k_R and k_{NR} represent the radiative and nonradiative decay constant, Φ is the quantum yield of the compound. k_R can be determined through the following equation,

$$k_R = \frac{\Phi}{\tau} \qquad [5]$$

2.5 Circular Dichroism (CD) spectrometry: The CD spectra were measured using a Chirascan Cd/2T spectrophotometer equipped with a thermostatically controlled cell holder. Protein concentration was used as 10μM for all the measurements. The far UV region was scanned in between 200 to 260nm with an average of three scanning with a bandwidth of 5nm.

The final spectra were obtained by subtracting the buffer contribution from the original sample spectra. The ellipticity MRE was calculated as follows.

$$\mathbf{MRE\ (deg\ cm^2\ dmol^{-1})} = \frac{\boldsymbol{\theta_{obs}}}{\mathbf{C_p nl\ \times 10}} \qquad [6]$$

Where, θ_{obs} is the observed ellipticity in mdeg, Cp is the molar concentration of the protein, n is the number of amino acid residues; l is the cell path-length.

The change in % helicity was then determined from the following equation.[44]

$$\%\ \boldsymbol{\alpha}\ \mathbf{Helix} = \frac{-(\mathbf{MRE} - \mathbf{2340})}{\mathbf{30300}} \times \mathbf{100} \qquad [7]$$

2.6 Protein corona study: To monitor the hard and soft corona formation around GNPs, time dependent DLS experiments were performed. GNP (0.64nM) and protein (10μM) in phosphate buffer (pH 7.4) were incubated at room temp. After incubation, the solution was centrifuged for approximately 10 minutes at 10000g, followed by pellet resuspension in the equal amount of exchanged solvent (water).

2.7 Fourier Transform Infra-Red Spectroscopy (FTIR): FTIR spectra of BSA and its conjugated systems with nanoparticles were measured using a Perkin-Elmer FTIR spectrophotometer equipped with a horizontal attenuated total reflectance (ATR) accessory containing a zinc selenide crystal and operating at 4 cm^{-1} resolution. The net BSA spectrum in solution was calculated by subtracting the solvent (water) spectrum from the solution spectrum. The use of this spectral subtraction provided reliable and reproducible results.

2.8 UV-VIS Optical spectroscopy: The UV VIS spectroscopy of GNPs and the conjugates were measured using Shimadzu UV Vis 2450 and Shimadzu UV Vis NIR 3600 spectrophotometer. The spectra were collected using a quartz cuvette with 10 mm path length.

2.9 Computer simulation

2.9.1 Surface Modifications of GNP (111)

The surface was modified by simply changing the coordinates in the PDBQT files.[14] The different surfactant molecules were added by adding their PDBQT coordinates and parameters to the PRBQT file of the gold surface. Molecules were aligned to the intended region with proper orientations. MATLAB7.10.0 and NOTEPAD++ were used to carry out all the coordinate transformation. The ligand was treated as a rigid entity. These molecules along with all other surfactant molecules were optimized by MGL Tools 1.5.4 by adding Marsilli-Gasteiger partial charges on each constituent atom.

2.9.2 Docking experiments

The MGL Tools 1.5.4 was used as a user interface to prepare the docking files and AutoGrid4 and AutoDock4 was used to carry out the grid and energy calculations respectively.[45-46] The new parameter library was used in both cases. The grid was set to the maximum size allowed by AutoDock which is 126 points in each three directions with 1 Angstrom grid spacing. This much of grid volume was to ensure that the gold surface can move freely around the small protein at the center. The standard AutoDock force fields were used for energy calculations while the best conformation was optimized by Lamarckian Genetic Algorithm (GA). With an initial population size of 150 and number of evaluation of 250000, the GA was allowed to run up to 27000 generations to find one best individual. Each of our experiments was set for 100 GA runs. The

gene mutation and crossover rate was taken 20% and 80% respectively. AutoDock Clustering were analyzed to know the nature of the simulation result, i.e., how well they were converging and what were the population size for each conformation.

3. Result and Discussion:

All the particles were characterized by using TEM, DLS and their corresponding surface plasmon bands **[Figure 1a-f].** The stability of the nanoparticles was further confirmed by measuring the Zeta potential[37] (**Table 1**). The inset of Figure 1e shows the respective SPR bands for a typical TGNP. The band at 570nm is due to transverse SPR and at 1307nm is due to the longitudinal SPR. The intensity correlation and the corresponding fit of the raw DLS data showed the dispersity and distribution of the nanoparticles. The data showed that the size of all the GNPs, majorly, appeared in between 43-46nm **(Supporting Figure S2**). Concentration of the nanoparticles was calculated by assuming that all the $HAuCl_4.3H_2O$ have been converted to nanoparticles.[47]

3.1 Steady state fluorescence changes on protein local microenvironment

Fluorescence spectroscopy is one of the most important techniques to understand the conformational changes of protein as it directly monitor the change in fluorescence properties of tryptophan moiety when attached to a nanoparticle.[48] BSA has two tryptophan moieties, Trp134 situated in subdomain IA and Trp 214 situated in the subdomain IIA. These can provide valuable information on the conformational changes upon complex formation.[49] Trp in BSA exhibits fluorescence emission at 345nm at pH 7.4 in PBS buffer when excited at 280nm.[50] Significant reduction in fluorescence intensity was observed when the concentration of nanoparticle increases [**Figure 2**]. No fluorescence signal was observed only for nanoparticle suggesting the

fluorescence changes were due to the nanoparticle protein conjugate systems **(Supporting Figure S3**). A 20 nm of blue shift in the emission maxima was observed in the presence of all CTAB stabilized GNPs. This signifies the symptomatic shift of the dielectric properties of the medium and consequently reduction of the polarity of the local environment of the fluorescent molecule due to local structural rearrangements. Interestingly, the citrate stabilized spherical GNP shows only quenching. No spectral shift was observed for this particle. This data suggests that the properties of surface ligands (charge, surface density and chain length) play major roles in the above spectral changes. BSA has the pKI of 4.7. As a result at the experimental pH (pH 7.4) BSA possesses a negative charge.[51] Hence, electrostatic repulsion between negatively charged citrate stabilized spherical GNP and negatively charged BSA should hinder the protein adsorption. However, in the present case strong interaction was observed. The strong binding of BSA to citrate stabilized spherical GNP is occurred most probably with the formation of salt bridges of the carboxylate ammonium type, between the citrate and the lysine on the protein surface.[52] On the other hand, though electrostatic interaction should favor the BSA binding to CTAB stabilized spherical GNP, but the mechanical strain of the hydrophobic chains of CTAB molecule hinders the protein to access the GNP surface. This has been discussed in a later section.

For a quantitative estimation of the above quenching, the fluorescence data were fitted using the Stern Volmer equation.[53]

$$\mathbf{F_0/F = 1 + K_{sv}[Q]} \qquad [8]$$

Where, F_0 and F denote the steady state fluorescence emission intensities in the absence and presence of the quencher, respectively. K_{sv} is the Stern–Volmer quenching constant and [Q] is the

concentration of GNPs. Data shows that the K_{sv} is maximum for citrate stabilized spherical GNP and minimum for TGNP (**Supporting Figure S4)**. The order of K_{sv} was as follows: citrate stabilized spherical GNP > CTAB stabilized spherical GNP> GNR>TGNP (**Table 2)**. The equilibrium binding constant and the number of binding sites between BSA and all different GNPs were also determined from the following equation.[54]

$$\log [(F_0 - F)/F] = \log K_b + n \log [Q] \qquad [9]$$

Where K_b is the equilibrium constant and n is the number of binding sites. [48,49] The values of K_b and n for all nanoparticles with BSA are shown in **Table 2 and Supporting Figure S5.** When n > 1, binding of a ligand is enhanced, provided, other ligands are adsorbed onto the surface. Similarly, when n < 1, binding strength of a ligand decreased. In cases where n = 1, the binding of a ligand is independent of the ligands, which are already present on the surface. [53] The order of binding constant (K_b) was also similar to $K_{sv.}$ Citrate stabilized spherical GNP > CTAB stabilized spherical GNP> GNR>TGNP. These results explicitly suggest that not only the surface functionalization but the particle morphology also plays a significant role in protein adsorption onto GNP surface.

3.2 Time resolved fluorescence on BSA GNP conjugates

Time resolved fluorescence measurement is a very important and sensitive technique to understand the effect of microenvironment surrounding a fluorescent molecule. The change in fluorescence lifetime of the tryptophan moiety of BSA while adsorbed onto the metal surface can

be explained by the fact that the proximity of the metal provides an additional pathway of de-excitation.[55]We have measured the fluorescence lifetime of BSA protein in the presence of the different GNPs **(Figure 3)**. The decay curve of free BSA was fitted biexponential with lifetime 3.87ns and 6.95ns. Recent studies have shown that the shorter lifetime is independent of any structure and is characterized as an internal property and organization of the tryptophan structure in the excited state.[56]The longer component of the lifetime is attributed to the interaction between tryptophan residue and the surrounding microenvironment of the protein. However, without going to the individual component, for simplicity we use the average lifetime as 6.35ns. The lifetime found to decrease substantially in the presence of all CTAB stabilized spherical nanoparticles **(Table 2)**. For citrate stabilized spherical GNP lifetime remains same as of free BSA. From the above data it could be concluded that the quenching of fluorescence in presence of all CTAB stabilized GNPs (TGNP, GNR and CTAB stabilized spherical GNP) are dynamic in nature while for citrate stabilized spherical GNP, it is static in nature.[57] From the above lifetime data, we finally calculated the radiative and non-radiative decay to find out the mechanism of the quenching. An extensive increase in the non-radiative decay rate for all the CTAB stabilized GNPs and an extensive decrease of the radiative decay rate for citrate stabilized spherical GNP was observed. So, the decreased in lifetime of tryptophan residues in protein in the presence of CTAB stabilized spherical GNPs is attributed to the decrease in the non-radiative decay rate. The lowering of the polarity around the tryptophan residue in protein environment observed from steady state (around 20nm blue shifting) is also reflected by the above decrease in lifetime.[58]

3.3 Red-edge excitation shift (REES)

Red edge excitation shift (REES) is the shifting of the emission maxima to the red end of the spectrum upon shifting of the excitation wavelength to the red end of the absorption spectra of the fluorophore.[59]This is a wavelength sensitive tool for directly monitoring the environment and dynamics around a fluorophore in a complex biological system. The more the change in the microenvironment of the surrounding probe, the more will be REES effect. **Figure 4** displays the REES measurements of tryptophan moiety of BSA in presence of different GNPs. It is observed that for all CTAB stabilized spherical GNPs, the shift of excitation wavelength from 280 to 310nm resulted in a shift of the emission maxima of the probe from 324 to 336nm (12 nm REES shift occurred in 10μM BSA). However, for citrate stabilized spherical GNPs, no change was observed.

This observation, therefore, explicitly suggests that binding of all the CTAB stabilized GNPs to BSA changes the microenvironment around tryptophan moiety as was also observed from the steady state fluorescence data, where 20nm blue shifting in the emission maxima was observed. It was interesting at this point to measure the REES data on denatured protein using guanidinium chloride (GdmCl), which induced unfolding of BSA in a two steps, three state transitions with accumulation of an intermediate (I) around 4-5 M GdmCl concentration.[60] Denaturation of BSA with increasing concentration of GdmCl resulted in greater exposure of the probe molecules to the aqueous buffer environment from the confined environment inside the protein backbone, a direct consequence of which is manifested through minimum or no REES after complete denaturation of the protein conformation **(Supporting Figure S6)**. All the above data supports the spectral shift in fluorescence.

3.4 Structural stability of GNP protein conjugates

It was very important at this stage to find out the structural effect and the binding stability of the GNPs to the protein. If the 3D structure of BSA is disrupted, the protein will merely bind to the nanoparticle surface. Hence a titration experiment was performed on the GNP protein conjugates with increasing denaturant GdmCl concentration. **Figure 5** displays the changes in the emission spectra of GNP protein conjugates with increasing concentration of GdmCl. The data showed that a gradual addition of the denaturant decreased the intensity of the tryptophan fluorescence along with the simultaneous red shift of the earlier obtained blue shifted emission maxima. These observations are in line with the idea that the protein binds to GNP in its native conformation, and denaturation of the earlier leads to the disturbance of that binding. We also performed a reverse experiment where initially the half and full denaturation condition of the protein was produced and then the GNPs were added to it. **Figure 6** shows that in half denaturation condition the blue shifting is still observed, though the amount of shifting is just half than that of observed in the native condition. However, interestingly, at full denaturation condition, no shifting was observed for any of the GNPs. This data exclusively suggested that at half denatured condition still there is a possibility of GNP binding as half of the structure is being lost however in a completely denatured condition the binding of GNP to protein is completely lost.

3.5 Agglomeration of protein nanoparticle conjugate

Previous reports suggest that the partial unfolding of the protein while adsorbed onto the nanoparticle surface may lead to agglomeration. For finer details about the structural stability

and any agglomeration of the conjugate systems, we performed various other experiments. Several mechanisms are proposed for the agglomeration of the proteins. Reports suggest that it is completely dependent on the size and the number of disulphide bonds present in a particular protein. For example, smaller protein like lysozyme where only 4 disulphide bonds are present, breaking 1-2 bonds may exclusively responsible for large perturbation. However, for larger protein like BSA, which contains 17 disulphide bonds, breaking of fewer bonds will affect less on the overall secondary structure.[61]The large aggregation in lysozyme in presence of GNP is reported mainly due to the electrostatic interaction, where positively charged lysozyme efficiently interacts with negatively charged gold nanoparticle. [62] On the other hand, the agglomeration of BSA was highly dependent on its native and denatured conformation. It was observed that the denatured BSA favors more aggregation than its native conformation, while α amylase or green fluorescent protein showed opposite behavior.[63] Reports also suggest that, instead of any agglomeration behavior, BSA forms only a monolayer (protein corona) while attached to GNP[64] In view of all these results**,** it was important to check the possibilities of agglomeration for the different BSA GNP conjugates. The DLS data shows that, when GNP interacts with the protein, it forms a corona like structure. Both hard corona (monolayer around GNP) and soft corona are formed.[4,65] The soft corona was removed out by centrifugation at 10000g, followed by pellet resuspension in the equal amount of exchanging water. In native form, the hydrodynamic diameter of citrate stabilized spherical GNP increased to approximately 20nm while for the CTAB stabilized spherical GNP showed around 10-12nm increment.[14] GNR and TGNP also showed around 10-12nm increment in hydrodynamic radius (**Table 3)**. Hence, our data suggested that no agglomeration of the conjugate systems, rather protein corona was formed in each case. This was further confirmed by their change in respective UV-VIS spectra

and TEM images **(Supporting Figure S7-S8).** When the BSA was fully denatured, no change in the hydrodynamic diameter of any GNPs was observed. This data suggested that at denaturation condition the protein is not able to adsorb on the GNP surface. Hence it could be concluded that protein, preferably bind to the GNPs in its native conformation (**Table 3).**

3.6 Circular Dichroism Spectroscopy on secondary structural changes

We measured the CD spectral changes to get information about the secondary structure changes of the BSA protein in the presence of different GNPs. The spectrum of an all α helical protein has two negative bands of almost similar magnitude at 222 and 208nm, and a positive band at ~ 190nm. The band at 222nm is related to the strong hydrogen-bonding environment of α helices and is relatively independent of their length. The spectrum of an all β sheet protein has, in general, a negative band at around 208 nm and a positive band between 195 - 200 nm.[66-67] The percentage of α-helicity was calculated from the mean molar residual ellipticity ($^{\theta}$MRE), which gives a direct quantitative measurement of loss of α-helical structure of a protein**. Figure 7** shows the far-UV CD spectrum of native BSA at pH 7.4. It exhibits two negative minima at 208 and 222nm.[68] Significant change in helicity were observed in the presence of all the CTAB stabilized spherical GNPs. Interestingly, for citrate stabilized spherical GNP, the helicity was found to be minimized (Supporting **Table S2**). Both the anisotropic GNPs (GNR and TGNP) show almost similar amount of helicity changes at the same concentration. At similar concentration for CTAB stabilized spherical GNP the CD band at 208 is completely lost suggesting the extensive loss of secondary structure **(Supporting Figure S9)**. CTAB stabilized spherical GNP shows almost similar amount of secondary structural changes to that of anisotropic GNPs, when the concentration was used one order of magnitude less. These data

exclusively suggest that the shapes of the GNPs and the surface functionalization play major roles in the protein adsorption as well as its structural changes. All these data are being interpreted using the newly established theoretical simulation method.[14]

3.7 FTIR spectra of BSA nanoparticles conjugate systems

The secondary structure perturbations were also confirmed by FTIR spectroscopy. There are two regions 1700–1600 $cm^{-1}$and 1550–1500 cm^{-1} in the spectrum, which are unique to the protein secondary structure, called as amides I and II bands. These provide valuable information on conformational changes of the protein when conjugated with the nanoparticles. The amide I band (C=O stretch) has a correlation with the secondary structure of protein, whereas the amide II is responsible for C-N stretch to N-H bends and indicative of the amount of protein adsorbed on surfaces. BSA bound to all the GNPs revealed less intense amide I and II peaks as compared to free BSA, suggesting the adsorption of the protein onto the GNP surface **(Supporting Figure S10).** However, only in the case of TGNP, GNR and CTAB stabilized spherical GNPs extent decrease in the peak intensity was observed as compared to citrate stabilized spherical GNP. This data explicitly suggest that in the presence of all CTAB stabilized GNPs large amount of conformational changes occurred as observed in the CD data.

3.8 Theoretical Simulation: A hypothesized model on protein GNP binding

To explain the above experimental results, a molecular model is proposed with the help of docking simulation, recently established in our group.[14, 69] A {111} flat gold surface (10nm × 7nm) mimicking the particle curvature of a GNP (more than 40nm diameter) was constructed. The surface ligands (considering rigid models of CTAB and citrate) were placed on top of the

surface. Docking simulation was performed using AutoDock 4.2 tools with a semi-empirical free-energy force field to evaluate conformations during docking. The chosen computational method, details surface construction and validation could be found elsewhere.[14] The main limitation of our simulation approach is to consider protein as a rigid entity though in reality the protein structure should change while adsorbing onto GNP surface.

However, considering the rigid approximation of protein structure, we were successfully able to explain qualitatively all the experimental data. BSA protein has a typical heart shaped with approximate dimension of 9 x 9 x 4 nm **(Supporting Figure S1).** Our simulation data show that BSA uses its IIIA subdomain with a nearly perpendicular orientation to attach onto a citrate Stabilized spherical flat {111} surface for the stable conformation with an effective increased thickness of approximately 9nm**.** However, on a CTAB layer, BSA may bind in a different orientation (parallel to the GNP surface, where the effective thickness increases of about 4-5nm **(Figure 8)**. The stability of protein on CTAB stabilized spherical GNP was found to be less as compared to citrate stabilized spherical one, as on a citrate layer BSA has minimum perturbation. On the other hand, on a CTAB layer, the protein binding is disturbed by the mechanical strain of the hydrophobic chain length. The similar phenomenon was also observed for human serum albumin, which is mainly due to the structural similarity with BSA.[14] Experimentally, we also observed strong binding constant in case of citrate stabilized spherical GNP. In this case, the size of the citrate is very small as compared to the CTAB molecule. The size of the citrate ion is 0.717nm and the CTAB ion is approx. 2.6nm.[70] Hence it is quite possible that in citrate stabilized spherical GNP, the protein will be in close contact to the nanoparticle surface, however, in CTAB stabilized spherical GNP the protein will be at least 2.6nm far away from the GNP surface (at least for initial interaction).

The efficiency of this fluorescence quenching depends on the distance between the chromophore and the quencher, strongly depends on the total number of proteins adsorbed onto the GNP surface and finally with the strong binding constant. Our simulation, suggest that in case of citrate stabilized spherical GNP both the tryptophan residues are farther away than that of a CTAB stabilized spherical GNP **(Supporting Figure S11)**. Hence, it could be expected that in case of CTAB stabilized spherical GNP the quenching will be more than that of citrate stabilized spherical GNP. It has been shown that in the citrate layer BSA adsorbed in a perpendicular orientation and on a CTAB layer it adsorbed in a parallel orientation to the surface. Considering the above two different orientations, mathematical calculation suggests that the maximum number of albumin proteins which can be accommodated on the GNP surface is almost double on a citrate layer than on a CTAB layer **(supporting information).** Further, both the experimental and docking simulation shows stronger binding of BSA in citrate stabilized spherical GNP than CTAB stabilized spherical GNPs. As a result the overall quenching will be much higher for citrate stabilized spherical GNPs than CTAB stabilized spherical GNP for the same concentration of protein. For GNR and TGNP the number of protein molecules adsorbed onto a surface was calculated from their surface area **(Supporting Information and Table S1)**. The calculated surface area for GNR and TGNP are almost equal but approximately half as compared to the CTAB stabilized spherical GNP. As a result, it is quite obvious that the number of adsorbed proteins for these two GNPs will be even less than the CTAB stabilized spherical GNP. Consequently, the quenching will be less for these two GNPs.

The observed blue shifting in the fluorescence maxima in case of all CTAB stabilized spherical GNPs are possible due to the presence of the surface ligand itself (CTAB). The citrate ion is a triple negative charge small organic molecule while CTAB contains a long hydrophobic tail

along with the positive hydrophilic head. To establish that the interaction of the hydrophobic tail of CTAB to tryptophan moiety makes its surrounding more hydrophobic and results blue shifting (**Figure 8 and Supporting Figure S11),** a control experiment was performed where the same fluorescence was monitored by changing the concentration of free CTAB molecules. It is merely possible that any CTAB will contribute from the solution as those were mostly removed from the solution by centrifugation and proper washing in the synthesis process. A 6nm blue shifting was observed for only CTAB molecules. Hence, the extra 14nm blue shift is solely contributed by the GNP attached CTAB molecule.

Finally, the changes in CD results also could be explained with the help of the molecular model. In case of citrate stabilized spherical GNP, the protein is attached to the GNP surface only with fewer numbers of amino acids of the III A domain, whereas in CTAB stabilized spherical GNPs, several amino acids from entire protein are attached causing internal strain. Hence it is much clearer that the CD spectral changes in case of CTAB stabilized spherical GNP is more than citrate stabilized spherical GNP. The extra loss of secondary structure in presence of CTAB stabilized spherical GNP could be explained with the help of a number of proteins adsorbed. Our calculation shows that the number of proteins adsorbed for CTAB stabilized spherical GNP is much higher than GNR and TGNP; therefore the total structural loss also will be higher.

3 CONCLUSION

Synthesizing GNR, TGNP and both citrate and CTAB stabilized spherical GNPs of approximately similar size, in this paper we demonstrated how the morphology and different surface chemistry of GNP influence the adsorption and binding affinity of BSA protein on nanoparticle surface. Our data suggested both the above parameters play very crucial roles on

binding and orientation of BSA on GNP surface. Local environmental changes around tryptophan moiety and the secondary structural losses were also highly influenced by them. Stronger binding as well as quenching of tryptophan fluorescence were observed on a citrate stabilized spherical GNPs than all CTAB stabilized GNPs. Our newly proposed simulation model explains all the experimental results.

ACKNOWLEDGMENT

The authors acknowledged the home institute (IIT Mandi) and Department of Science and Technology (DST) India for their financial support (Project No: IITM/SG/CKN/003 and SR/FT/CS-152/2011) for running the docking simulations and experiments. The authors acknowledge to Dr. Samrat Mukhopadhyay and Mr. Dominic Narang, IISER Mohali India for using their CD facility.

REFERENCES

1. M. P, Monopoli, C. Aberg, A. Salvati and K. A. Dawson, *Nat. Nanotechnol* 2012**, 7** (12), 779-786.
2. Z. J. Deng, M. Liang, M. Monteiro, I. Toth and R. F. Minchin, *Nat. nanotechnol* 2010**, 6** (1), 39-44.
3. A. Salvati, A. S. Pitek, M. P. Monopoli, K. Prapainop, F. B. Bombelli, D. R. Hristov, P. M. Kelly, C. Aberg, E. Mahon and K. A. Dawson, *Nat. Nanotechnol* 2013**, 8** (2), 137-143.
4. E. Casals, T. Pfaller, A. Duschl, G. J. Oostingh and V. Puntes, *ACS Nano* 2010**, 4**, 3623–3632.
5. M. Lundqvist, J. Stigler, G. Elia, I. Lynch, T. Cedervall and K. A. Dawson, *Proc. Natl. Acad. Sci.* 2008**, 105,** 14265-14270.
6. C. A. Poland, R. Duffin, I. Kinloch, A. Maynard, W. A. Wallace, A. Seaton, V. Stone, S. Brown, W. MacNee and K. Donaldson, *Nat. Nanotechnol.* 2008**, 3** (7), 423-428.
7. J. S. Gebauer, M. Malissek, S. Simon, S. K. Knauer, M. Maskos, R. H. Stauber, W. Peukert and L. Treuel, *Langmuir* 2012**, 28** (25), 9673-9679.
8. M. E. A. Tam, W. Hwang and K. H.Schifferli, *Proc Natl Acad Sci U S A.* 2009**, 106** (11), 4095-4100.
9. S. G. Lopez, J. Juarez, M. A. Meda, E. Casals, V. F. Puntes, P. Taboada and V. Mosquera, *Langmuir* 2012, **28** (24), 9113-9126.
10. S. Shrivastava, J. H. Nuffer, R. W. Siegel and J. S. Dordick, *Nanolett.* 2012, **12** (3), 1583-1587.

11. Z.O. Araci, A F. Runge, W.J. Doherty and S. S. Saavedra, *J. Am. Chem. Soc.* 2008, **130** (5), 1572-1573.

12. H.S. Mandal and H. B. Kraatz, *J.Am. Chem. Soc.* 2007**, 129** (20), 6356-6357.

13. Z. J. Deng, M. Liang, I. Toth, M. J. Monteiro and R. F Minchin *ACS Nano* 2012, **6** (10), 8962-8969.

14. S. Khan, A. Gupta, and C. K. Nandi, *J. Phys. Chem. Lett. ,* 2013**, 4** (21), 3747-3752.

15. J. V. Jokerst and J. T. McDevitt, *Nanomedicine* 2010, **5** (1), 143-155.

16. T. Cha, A. Guo and X. Y. Zhu, *Proteomics,* 2005, **5** (2), 416-419.

17. M. Karlsson and U. Carlsson, *Biophys. J.* 2005, **88** (5), 3536-3544.

18. J. H. Nuffer and R. W. Siegel, *Tissue Eng. Part A* 2009**, 16** (2), 423-430.

19. G. MacBeath and S. L. Schreiber, *Science* 2000, **289** (5485), 1760-1763.

20. R. Singhvi, A. Kumar, G. P. Lopez, G. N. Stephanopoulos, D. Wang, G. M. Whitesides and D. E. Ingber, *Science* 1994, **264** (5159), 696-698.

21. E. C. Cho, L. Au, Q. Zhang and Y. Xia, *Small* 2010, **6** (4), 517-522.

22. W. Jiang, B. Y. Kim, J. T. Rutka and W. C. Chan, *Nat. Nanotechnol.*2008, **3** (3), 145-150.

23. P. Nativo, I. A. Prior and M. Brust, *ACS nano* 2008, **2** (8), 1639-1644.

24. J. E. Gagner, M. D. Lopez, J. S. Dordick and R. W. Siegel, *Biomaterials* 2011, **32** (29), 7241-7252.

25. J. E. Gagner, X. Qian, M. M. Lopez, J. S. Dordick and R. W. Siegel, *Biomaterials* 2012, **33,** 8503.

26. C.C. Chen, Y.P. Lin, C.W. Wang, H.C. Tzeng, C.H. Wu, Y.C. Chen, C.P. Chen, L.C. Chen and Y.C. Wu, *J. Am. Chem. Soc.* 2006, **128** (11), 3709-3715.

27. X. Huang, I. H. El Sayed, W. Qian and M. A. El Sayed. *J. Am. Chem. Soc.*2006, **128** (6), 2115-2120.

28. A. Wijaya, S. B. Schaffer, I. G. Pallares and K. H. Schifferli, *ACS nano* 2009, **3** (1), 80-86.

29. C. Bao, N. Beziere, P. del Pino, B. Pelaz, G. Estrada, F. Tian, V. Ntziachristos, J. M. de la Fuente and D. Cui, *Small* 2013, **9** (1), 68-74.

30. B. Pelaz, V. Grazu, A. Ibarra, C. Magen, P. del Pino, and J. M. de la Fuente, *Langmuir* 2012, **28** (24), 8965-8970.

31. J. E. Millstone, G. S. Métraux and C. A. Mirkin, *Adv. Funct. Mater.* 2006, **16** (9), 1209-1214.

32. J. E. Millstone, D-. G. Georganopoulou, X. Xu, W. Wei, S. Li, and C. A. Mirkin, *Small* 2008**, 4** (12), 2176-2180.

33. S. D. Medina, J. Blankenburg, J. Olson, C. F. Landes and S. Link, *ACS Sustain Chem Eng.* 2013, **1** (7), 833–842.

34. T. Chakraborty, I .Chakraborty, S. P. Moulik and S. Ghosh, *Langmuir* 2009, **25** (5), 3062-3074.

35. A. Das, R. Chitra, R. Choudhury and M. Ramanadham, *Pramana* 2004, **63** (2), 363-368.

36. D.H. Tsai, F. W. DelRio, A. M. Keene, K. M. Tyner, R. I. MacCuspie, T. J. Cho, M. R. Zachariah and V. A. Hackley, *Langmuir* 2011, **27** (6), 2464-2477.

37. S. Jana, S. Ghosh, S. Dalapati and N. Guchhait, *Photochem Photobiol Sci.* 2012, **11** (2), 323-332.

38. T. Sen, K. K. Sen, and A. Patra, *J. Phys. Chem. C* 2008, **112** (46), 17945-17951.

39. J. Kimling, M. Maier, B. Okenve, V. Kotaidis, H. Ballot and A. Plech, Turkevich , *J. Phys. Chem. B* 2006, **110** (32), 15700-15707.

40. R. Narayanan, R. J. Lipert and M. D Porter, *Anal. chem.* 2008, **80** (6), 2265-2271.

41. S. Hong, Y. Choi and S. Park, *Chemistry of Materials* 2011, **23** (24), 5375-5378.

42. S. Park, N. Sinha and K. H. Schifferli, *Langmuir* 2010, **26** (16), 13071-13075.

43. J. R. Lakowicz, *Springer*; *Principles of Fluorescence Spectroscopy,* New York 2006, **3**.

44. Y. J. Hu, Y. O. Yang, C. M. Dai, Y. Liu and X. H. Xiao, *Biomacromolecules* 2010**, 11**, 106-112.

45. G. M. Morris, R. Huey, W. Lindstrom, M. F. Sanner, R,- K. Belew, D. S. Goodsell and A. J Olson, *J. Comput. Chem.* 2009, **30,** 2785-2791.

46. R. Huey, G. M. Morris, A. J. Olson and D. S. Goodsell, *J. Comput. Chem*. 2007, **28,** 1145-1652.

47. W. Haiss, N. T. Thanh, J. Aveyard and D. G. Fernig, *Analytical chemistry* 2007, **79,** 4215-4221.

48. S. H. D. P. Lacerda, J.J. Park, C. Meuse, D. Pristinski, M.L. Becker, A. Karim and J.F. Douglas, *ACS Nano* 2010, **4**, 365-369.

49. E. Gelamo, C. Silva, H. Imasato and M. Tabak, *Biochim. Biophys. Acta, Proteins Proteomics.* 2002, **1594** (1), 84-99.

50. A. Papadopoulou, R. J. Green and R. A. Frazier, *J. Agric. Food Chem* 2005, **53** (1), 158-163.

51. W. M. de Vos, P. M. Biesheuvel, A. de Keizer, J. M. Kleijn and M. A. Cohen Stuart, *Langmuir* 2008, **24**, 6575-6584.

52. S. H. Brewer, W. R. Glomm, M. C. Johnson, M. K. Knag and S. Franzen, *Langmuir* 2005, **21**, 9303-9307.

53. S. P. Boulos, T. A. Davis, J. A. Yang, S. E. Lohse, A. M. Alkilany, L. A. Holland and C. J. Murphy *Langmuir* 2013, **29**, 14984-14996.

54. B. Pan, D. Cui, P. Xu, Q. Li, T. Huang, R. Heand and F. Gao, *Colloids Surf A Physicochem Eng Asp* 2007, **295** (1), 217-222.

55. M. Ranjan Gartia, J. P. Eichorst, R. M. Clegg and G. Logan Liu, *Appl. Phys. Lett.* 2012, **101** (2), 023118-023118-5.

56. M. R. Rainbow, S. Atherton and R. C. Eberhart, *J Biomed Mater Res* 1987, **21** (5), 539-555.

57. D. Gao, Y. Tian, S. Bi, Y. Chen, A. Yu and H. Zhang, *Spectrochimica Acta Part A* 2005, **62**, 1203–1208.

58. B. Ojha, and G. Das, *Chem. Comm*. 2010, **46,** 2079-2081.

59. B. K. Paul, A. Samanta, and N. Guchhait, *J. Phys. Chem. B* 2010, **114***,* 6183-6196.

60. B. Ahmad, M. K. A. Khan, S. K. Haq, and R. H. Khan, *Biochem. Biophys. Res. Comm.* 2004, **31** (1), 166-173.

61. D. Zhang, O. Neumann, H. Wang, V. M. Yuwono, A. Barhoumi, M. Perham, J. D. Hartgerink, P. W.Stafshede and N. J. Halas. *Nano Lett.*, 2009, **9** (2), 666–671

62. R. Khandelia, A. Jaiswal, S. S. Ghosh and A. Chattopadhyay. *Small* 2013, **9** (20), 3494-3505.

63. J. Deka, A. Paul and A. Chattopadhyay, *J. Phys. Chem. C*, 2009, **113** (17), 6936–6947.

64. S. D. Medina, S. McDonough, P. Swanglap, C. F. Landes, and S. Link *Langmuir*, 2012, **28** (24), 9131–9139.

65. T Cedervall, I. Lynch, M. Foy, T. Berggård, S. C. Donnelly, G. Cagney, S. Linse and K. A. Dawson, *Angew. Chem. Int. Ed.* 2007, **46** (30), 5754-5756.

66. N. J. Greenfield, *Nat. Protocols* 2007, **1** (6), 2876-2890.

67. N. Sreeramaa, S. Y. Venyaminovb and R. W. Woodya, *Anal. Biochem.* 2000, **287** (2), 243–251.

68. B. K. Paul, D. Ray and N. Guchhait, *Phys. Chem. Chem. Phys.*2012, **14** (25), 8892-8902.

69. S. Khan and C. K. Nandi, *Nanotechnol Rev.* 2014*, DOI 10.1515/ntrev-2014-0002.*

70. T. Huang, P. D. Nallathamby and X. H. N. Xu, *J Am Chem Soc.*2008,**130** (50), 17095–17105.

Table 1. Size distributions of the all GNPs using DLS and TEM characterization and their respective Zeta-Potentials. For calculating GNPs average size/ mean diameter, around sixty nanoparticles taken from each TEM image.

GNPs	**Conc.**	**D_H (nm)**	**TEM Size (nm)**	**Zeta potential (mV)**
BSA	10μM	9.5 (±0.5)	----------	----------
TGNP	38nM	46.1 (±2)	43.3 (±3.2)	+79.6
GNR	18nM	44.5 (±3)	39.7 (±3.7)	+69.9
CTAB stabilized spherical GNPs	1.6nM	43.8 (±3.5)	40.2 (±3.4)	+37.1
Citrate stabilized spherical GNPs	1.6nM	43.7 (±4)	40.9 (±3.1)	-29.9

Table 2. Different parameters of BSA protein in presence or absence of GNPs calculated from the fluorescence data. Q represents the quantum yield, k_R and k_{NR} are the radiative and nonradiative decay, % k_R and % k_{NR} are the changes in the respective decay rate when GNP protein conjugate is formed, K_{sv} and K_b are the Stern Volmer quenching and binding constants. n is the number of binding site and ɽ is the lifetime.

BSA + GNPs	**Q**	**k_R**	**% k_R**	**k_{NR}**	**% k_{NR}**	**K_{sv}**	**K_b**	**n**	**Lifetime (ɽ in ns)**
BSA	0.129	0.020	--------	0.137	----------	----------	----------	-------	6.35
BSA + TGNP	0.065	0.0165	17.5	0.237	72.9	$6.9x10^7$	1.46×10^8	0.599	3.93
BSA + GNR	0.0505	0.0151	14.5	0.284	107.2	$2.8 x10^8$	$2.24x10^8$	1.10	3.34
BSA + CTAB stabilized spherical GNPs	0.0853	0.0217	8.5	0.233	70.7	$3.38x10^8$	$3.62x10^8$	0.546	3.92
BSA + Citrate stabilized spherical GNPs	0.062	0.0098	51	0.148	8.02	$2.34x10^9$	$2.57x10^9$	1.35	6.32

Table 3. Changes in the hydrodynamic diameter (D_H) of all the GNPs, when BSA adsorbed onto its surface. The data are shown for BSA in its native, half denatured and full denatured condition.

GNPs	Only BSA Size (nm)	GNPs (D_H) (nm)	BSA + GNPs (Native) (nm)	BSA + GNPs (Half denatured) (nm)	BSA + GNPs (Full denatured) (nm)
TGNP	9.5 (±0.5)	46.1 (±2)	57	52	47
GNR	9.5 (±0.5)	44.5 (±3)	55	48	46
CTAB stabilized spherical GNPs	9.5 (±0.5)	43.8 (±3.5)	54	49	46
Citrate stabilized spherical GNPs	9.5 (±0.5)	43.7 (±4)	64	49	46

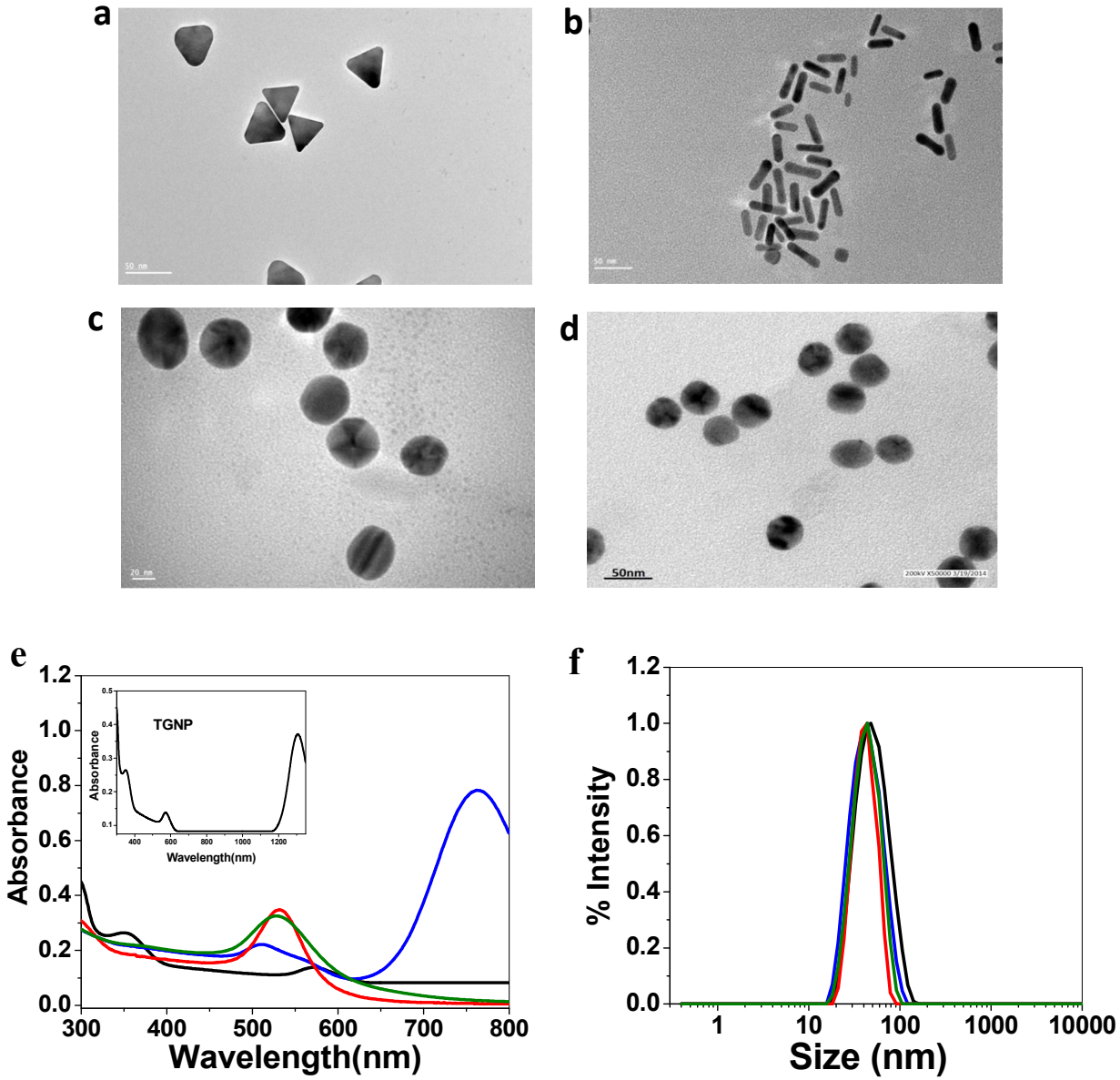

Fig. 1 Characterization of different shaped gold nanoparticles. TEM images of (a) TGNP, (b) GNR, (c) CTAB stabilized spherical GNP and (d) citrate stabilized spherical GNP; (e) UV VIS NIR Spectra of synthesized nanoparticles (TGNP in black, GNR in blue, CTAB stabilized spherical GNP in red and citrate stabilized spherical GNP is in green color), Inset shows the UV VIS NIR spectrum of TGNP; (f) DLS data of all GNPs.

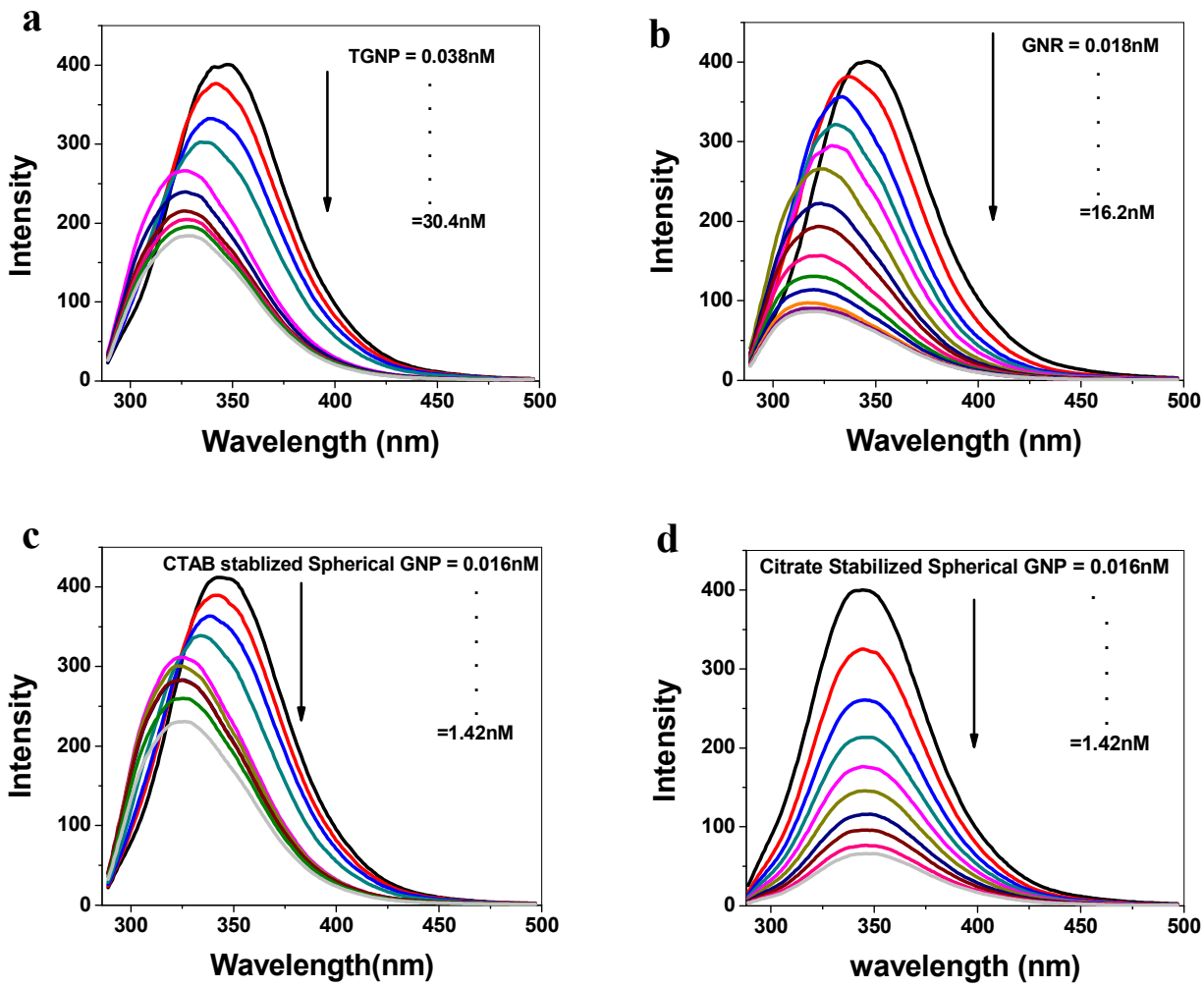

Fig. 2 Fluorescence titration emission spectra of BSA GNPs conjugates with increasing concentrations of GNPs (a) BSA- TGNP (b) BSA - GNR (c) BSA- CTAB stabilized spherical GNP, (d) BSA- citrate stabilized Spherical.

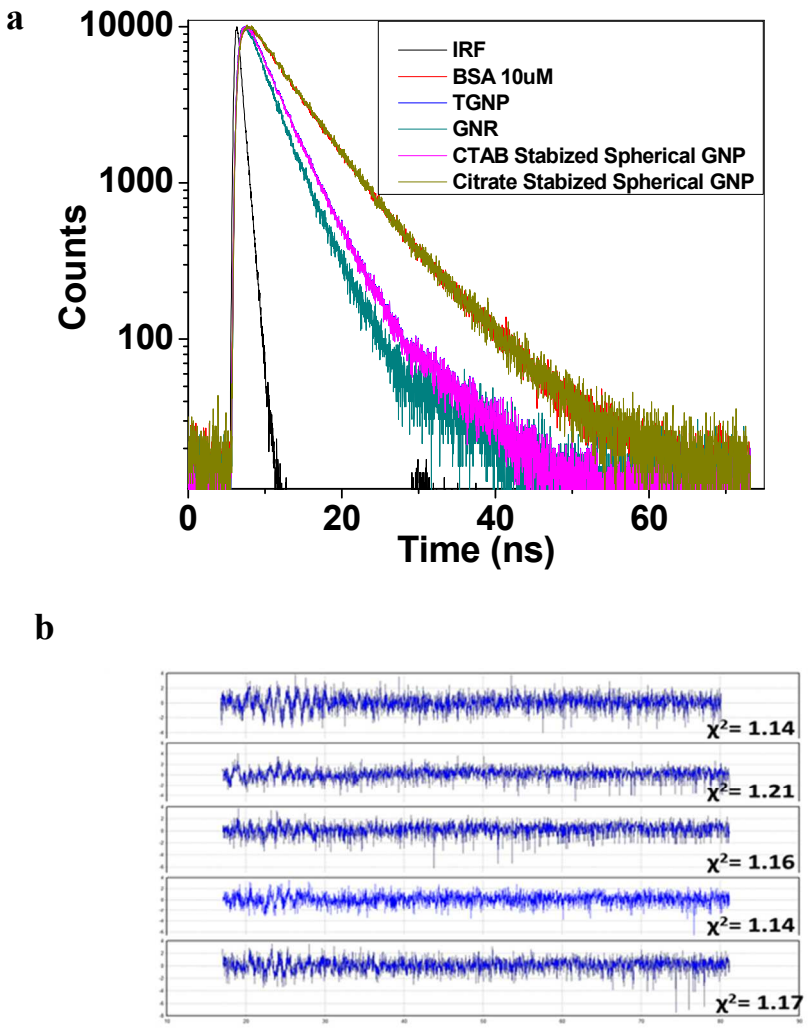

Fig. 3 a) Time-resolved fluorescence decay profiles of only BSA (red color) and in the presence of different GNPs (TGNP in blue color, GNR in green color, CTAB stabilized spherical GNP in pink color and citrate stabilized spherical GNP in olive green); b) the chi square fitting of the decay data.

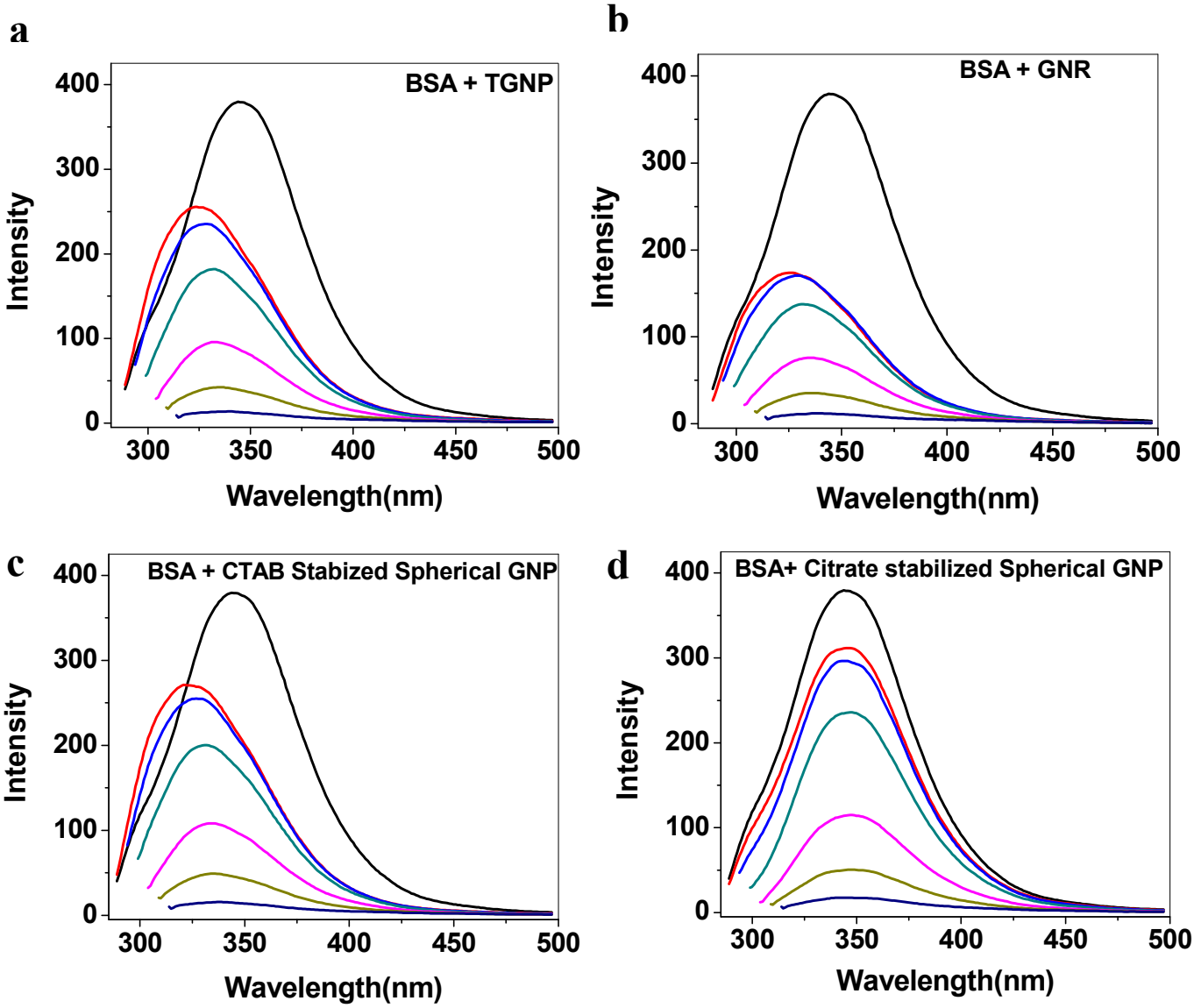

Fig. 4 REES results for native BSA in presence of a) TGNP b) GNR c) CTAB stabilized spherical GNP and d) citrate stabilized spherical GNP. A free BSA fluorescence spectrum is in black color in all figures. The different excitation modes are shown as follows: excitation at 280nm in red, at 285nm in blue, at 290nm in green, at 295nm in pink, at 300nm in olive green and at 305nm in navy blue color.

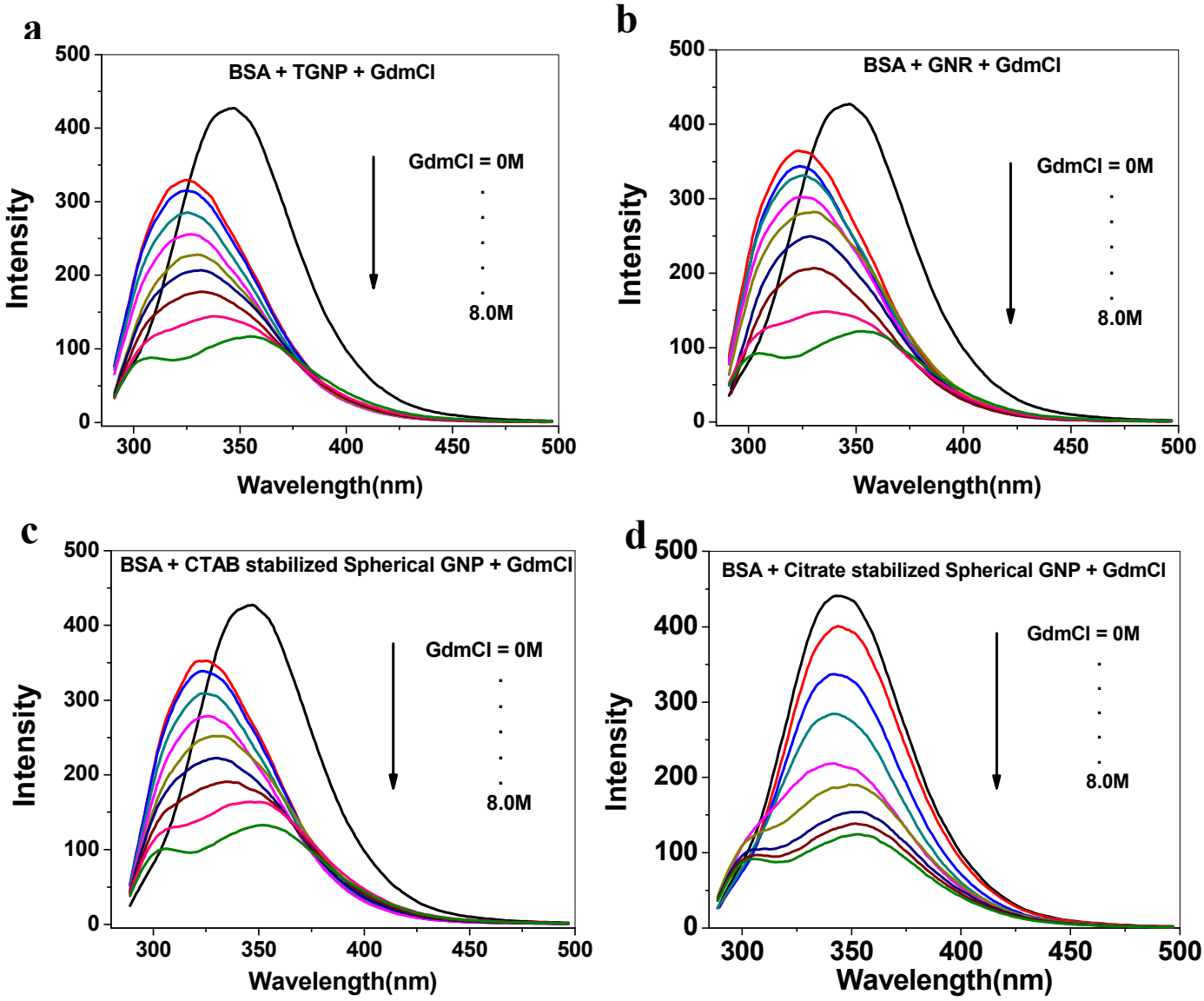

Fig. 5 Effect of denaturation on the BSA GNP conjugates a) TGNP b) GNR c) CTAB stabilized spherical GNP and d) citrate stabilized spherical GNP (fluorescence changes from red to green color represents the corresponding addition of GdmCl from 0M to 8.0M).

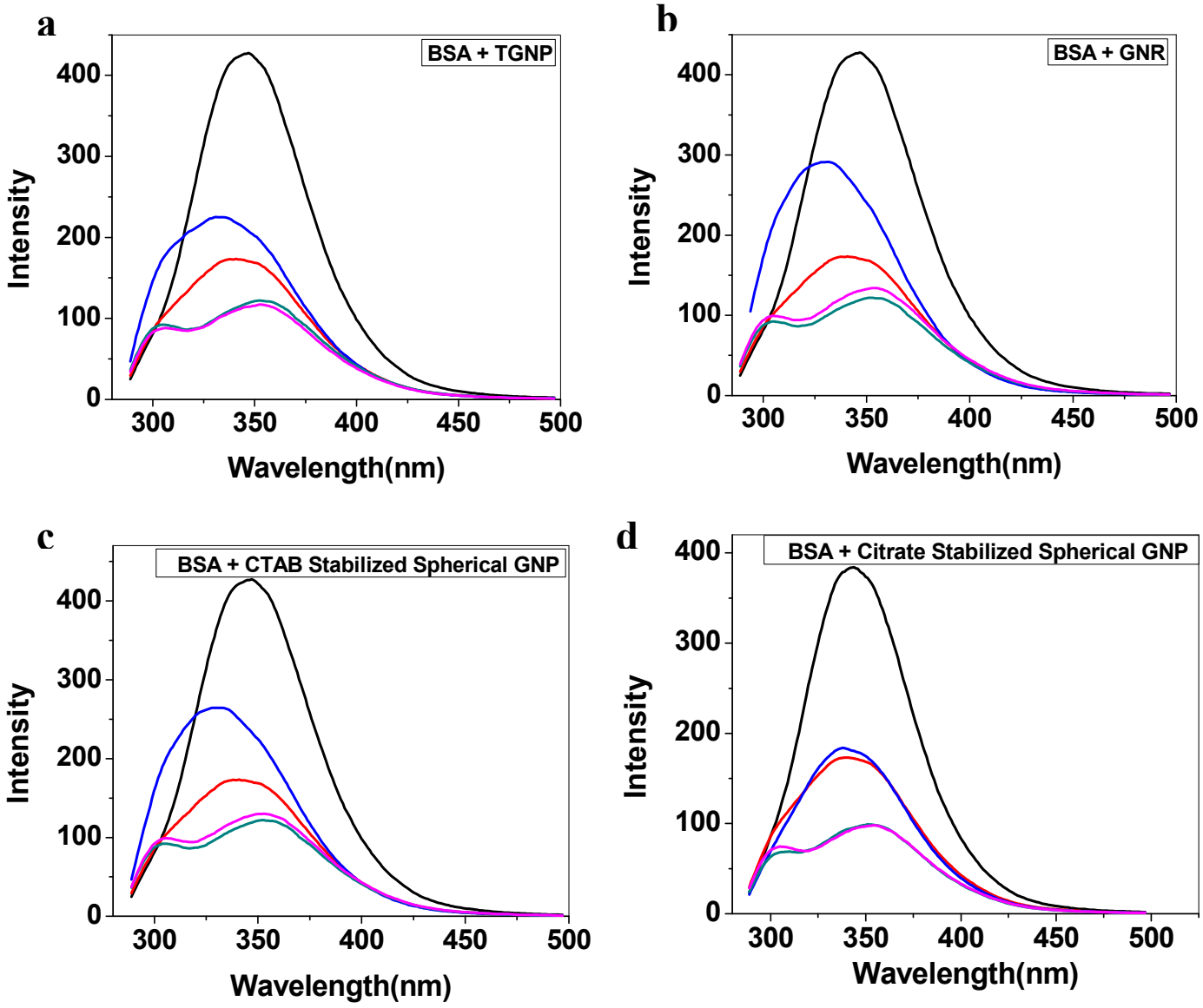

Fig. 6 The results showed that the amount of blue shifting is approximately half and zero at half and full denaturation condition of BSA. a) TGNP b) GNR c) CTAB stabilized spherical GNP. This data suggest that the amount of complex formation is reduced with increasing the concentration of denaturant; d) citrate stabilized spherical GNP shows no changes in either condition. BSA in black, BSA at half denatured condition in red, BSA at half denatured condition + GNP in blue, BSA at full denatured in green and BSA at full denatured condition + GNP in pink color.

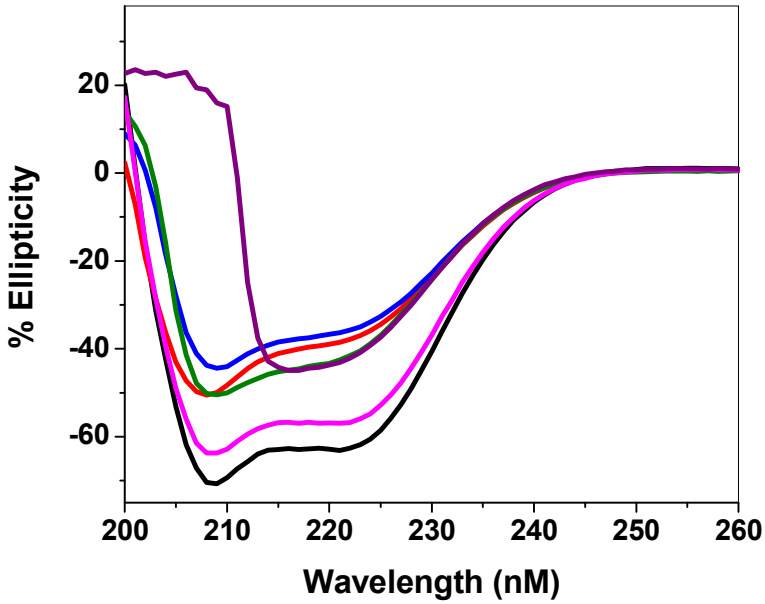

Fig. 7 Circular Dichroism spectra of BSA protein in presence of different GNPs. The data show minimum helicity changes for citrate stabilized spherical GNP. Almost equal amount of changes in helicity was observed for both the anisotropic GNR and TGNP at the same concentration. CTAB stabilized spherical GNP shows loss of the native structure is almost similar when the concentration was one order magnitude less. (Color representations are as follows: BSA- black, 1.6nM TGNP in red, 1.6nM GNR in blue, 0.16nM CTAB stabilized spherical GNP in green, 1.6nM citrate stabilized spherical GNP in pink, 1.6nM CTAB stabilized spherical GNP in violet).

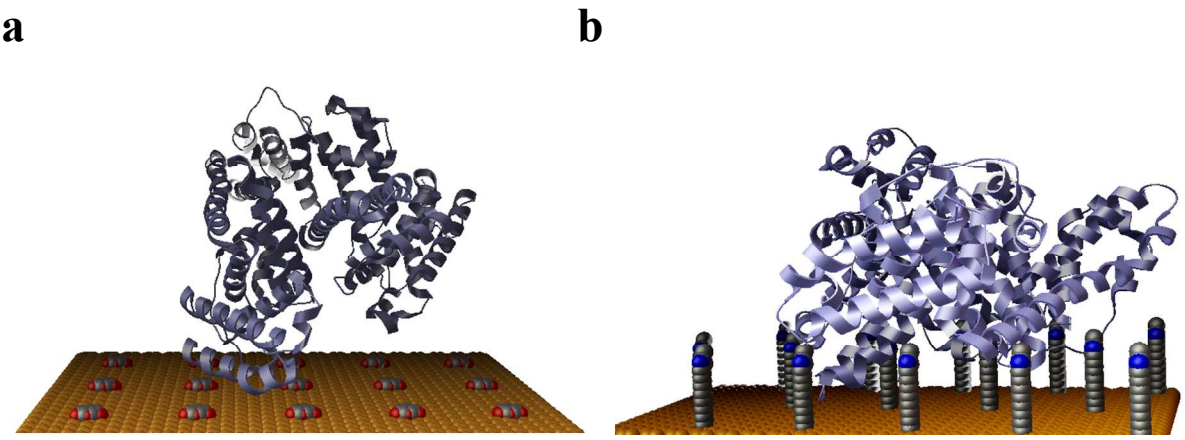

Fig. 8 Theoretical simulations of BSA protein on a) citrate stabilized spherical GNP and b) on a CTAB stabilized spherical GNP of similar size.